A Stepwise Downscaling Method for Generating High-Resolution Land Surface Temperature From AMSR-E Data

Quan Zhang, Ninglian Wang, Jie Cheng, *Senior Member, IEEE*, and Shuo Xu

***Abstract*—A stepwise downscaling method is proposed for generating high-resolution land surface temperature (LST) from advanced microwave scanning radiometer for the Earth observing system (AMSR-E) data to benefit the fusion of thermal infrared and microwave data for high-quality all-weather LST. This method sets a series of intermediate resolution levels between the initial (0.25°) and target (0.01°) resolutions, then downscales AMSR-E LST from one resolution to the next one step at a time, starting from 0.25° and ending with 0.01°. The geographically weighted regression model is adopted in each step to construct the relationship between LST and environmental variables, including normalized differential vegetation index, elevation, and slope. The stepwise method is verified over three regions in China that represent different characteristics of landscape heterogeneity varying from the highest to the lowest: the Yunnan-Guizhou Plateau (YGP), the border of Shanxi Province and Henan Province (BSH), and the central part of Inner Mongolia (CIM). Verified using the emulated AMSR-E LST resampled from reference MODIS LST available in 2010, the results show that the proportions of dates when the stepwise method is better are 100%, 78.1%, and 51.5% in the YGP, BSH, and CIM regions, respectively, which means the stepwise method has an advantage over the direct method in the regions with high heterogeneity. For real AMSR-E LST, the downscaled LST exhibits a similar spatial pattern to that of emulated data but suffers from reduced accuracy and contrast, which is caused by the smooth spatial pattern and low accuracy of the real AMSR-E LST.**

***Index Terms*—Downscaling, geographically weighted regression, land surface temperature (LST), microwave, scale effect.**

Manuscript received May 22, 2020; revised July 20, 2020 and August 13, 2020; accepted September 1, 2020. Date of publication September 9, 2020; date of current version September 30, 2020. This work was supported in part by the National Natural Science Foundation of China under Grant 41771365, in part by the National Key Research and Development Program of China under Grant 2016YFA0600101, and in part by the Strategic Priority Research Program of the Chinese Academy of Sciences under Grant XDA19070302. *(Corresponding author: Jie Cheng.)*

Quan Zhang is with the Shaanxi Key Laboratory of Earth Surface System and Environmental Carrying Capacity, the Institute of Earth Surface System and Hazards, College of Urban and Environmental Science, Northwest University, Xi'an 710127, China, and also with the State Key Laboratory of Remote Sensing Science, Faculty of Geographical Science, Beijing Normal University, Beijing 100875, China (e-mail: zhangquanzq@126.com).

Ninglian Wang is with the Shaanxi Key Laboratory of Earth Surface System and Environmental Carrying Capacity, the Institute of Earth Surface System and Hazards, College of Urban and Environmental Science, Northwest University, Xi'an 710127, China, and also with the CAS Center for Excellence in Tibetan Plateau Earth Sciences, Beijing 100101, China (e-mail: nlwang@nwu.edu.cn).

Jie Cheng and Shuo Xu are with the State Key Laboratory of Remote Sensing Science, Faculty of Geographical Science, Beijing Normal University, Beijing 100875, China (e-mail: jie_cheng@bnu.edu.cn; 365428302@qq.com).

Digital Object Identifier 10.1109/JSTARS.2020.3022997

I. Introduction

LAND surface temperature (LST) is one of the critical indicators that gauge the energy balance and material exchange near the Earth's surface, which is extensively applied in the fields such as evapotranspiration estimation, crop yield estimation, urban heat island research, hydrologic cycle research, vegetation monitoring, and disaster prediction [1]–[7]. Remote sensing is a unique means for obtaining LST over large spatial scales. The satellite LST retrieval methods can be divided into thermal infrared (TIR) and microwave (MW) algorithms in view of the spectral range. TIR algorithms are recognized as much more developed, and the retrieved LST has a relatively high spatial resolution and accuracy [8]–[10]. However, the TIR signal is sensitive to the atmosphere and cannot penetrate clouds, which prevents onboard sensors from capturing information from the land surface and leads to serious missing data problems in the LST products [11], [12]. In contrast, MW signals can penetrate clouds and compensate the defect of spatial integrity in TIR data. However, the resolution and accuracy of MW LST are generally lower than those of TIR [13]. The respective drawbacks of TIR and MW data hinder the single-source LST product from meeting the higher quality requirement in various fields [14], [15]; therefore, it is urgent to develop methods that can obtain LST data with high spatial resolution and high accuracy under all-weather condition simultaneously.

Research on the fusion of TIR and MW LSTs to generate high quality all-weather LST has drawn much attention in recent years [16]–[21]. Current studies show that the fusion of TIR and MW LSTs combines the advantages of these two data types, making it possible to obtain high quality all-weather LST. However, although the fusion methods have basically achieved all-weather coverage, the accuracy of the data filling in the cloudy area is still lower than that obtained under clear sky conditions. The major cause of this deficiency is that there is a large gap of accuracy and spatial scale between the filling source (i.e. MW LST) and TIR LST. Many studies have focused on the development of MW LST retrieval algorithms and the accuracy of retrieved MW LST has obviously improved [22]–[29]; however, few studies have paid attention to its spatial scale difference with TIR LST.

LST downscaling is an effective way to reduce the scale difference by enhancing low-resolution LST using spatially distributed auxiliary data that are statistically correlated to LST [30]. The auxiliary data are commonly called scaling factors

[31]. The downscaling of LST in most studies is realized by constructing the regression relationship between LST and the scaling factors. Although this relationship necessarily varies across scales, and the larger the scale difference, the greater the scale effect of the relationship [32], it is well accepted that applying regression models to small scale differences can weaken the impact of scale effect on LST downscaling. The current downscaling methods are all based on the assumption that this relationship is unchanged across the scales due to the complexity of scale effect and the relatively small difference of resolutions before and after downscaling. The basic framework of most downscaling methods are the same: construct the regression model between LST and scaling factors at the initial resolution (i.e., the resolution of the original LST data), and then apply the model to the scaling factors at the target resolution (i.e., the resolution of the downscaled LST) to estimate the downscaled LST. Scaling factor, regression model, and spatial resolution are the key elements in LST downscaling, so that the relevant studies are concentrated on these three elements.

The vegetation-related parameters, including the normalized differential vegetation index (NDVI) and fractional vegetation cover (FVC), are the earliest and most widely adopted scaling factors [33], [34]; however, this type of parameter cannot satisfy all the environmental conditions due to the complexity of landscapes. The LST downscaling methods designed for different landscapes have therefore been proposed [31], [35]–[38]. Scaling factors including emissivity [39], albedo [40], land cover type [41], digital elevation model (DEM) [42]–[44], soil-adjusted vegetation index (SAVI), normalized multiband drought index (NMDI), normalized difference water index (NDWI), and normalized difference build-up index (NDBI) [38] are fed into the regression models in different combinations.

The regression models can be divided into simple ones and complex ones. The simple models primarily include univariate or multivariate regressions, and linear, nonlinear, or piecewise linear regressions [32]–[34], [45]. These kinds of methods are generally suitable for the cases of fewer scaling factors or more homogeneous surface environments. For the situation with more scaling factors, Zakšek and Oštir [36] proposed a method, "downscaling," based on principal component analysis (PCA) to reduce the information redundancy among the scaling factors. The complex models primarily include the cokriging interpolation model [46], [47], the geographically weighted regression (GWR) model [42], the random forest (RF) model [44], and the artificial neural network (ANN) model [48], [49]. These kinds of models allow for the fact that the relationship between LST and scaling factors changes spatially, and they use local regression or classification strategies to achieve the LST downscaling.

To date, the current downscaling models are primarily aimed at TIR LST data from moderate to high resolution because of their more extensive applications, and relatively small difference between initial and target resolutions, commonly ranging from 2 to 10 times. Examples are the downscaling of the Spinning Enhanced Visible and Infrared Imager (SEVIRI) LST from 5 km to 1 km [36], the MODIS LST from 1 km to 250 m or 90 m [32], [42], [43], and the Thematic Mapper (TM) LST from 120 m or 60 m to 30 m [34]. In contrast, except for some downscaling processes of MW brightness temperatures in retrieving soil moisture [50], [51], there are few special studies on the downscaling of MW LST due to its lower resolution compared with TIR LST. The development of fusion methods for TIR and MW LSTs has increased the demand for MW LST downscaling. At present, a few cases of MW LST downscaling processes are integrated in the study of TIR and MW LSTs fusion methods [18], [19], but these processes are simplistic or not specifically designed for MW LST. Generally, the study of MW LST downscaling is in an early stage of development.

The main difference in downscaling between MW and TIR LSTs is their initial and target resolutions. For example, to fuse with MODIS LST, advanced microwave scanning radiometer for the Earth observing system (AMSR-E) LST should be downscaled from 0.25° (approximately 25 km) to 0.01° (approximately 1 km). These two resolutions differ by about 25 times, which is obviously larger than that in TIR LST downscaling. The scale effect would significantly impact the accuracy of downscaled MW LST if the regression relationship is applied under such a large scale difference. To weaken the scale effect in MW LST downscaling, this study proposes a stepwise downscaling method for AMSR-E LST. First, a resolution series was defined by incorporating two intermediate resolutions (0.08°, 0.03°) between the initial (0.25°) and target (0.01°) resolutions; then GWR was taken as the regression model and NDVI and DEM were taken as the scaling factors to downscale AMSR-E LST from 0.25° to 0.01° passing through the intermediate resolutions. The introduction of intermediate resolutions ensures the regression model is used in a relatively small resolution difference before and after each stepwise downscaling process of MW LST, which is similar to that in TIR LST downscaling. The stepwise method was expected to obtain a higher accuracy of downscaled MW LST and enhance the performance of TIR and MW LSTs fusion procedures.

II. Study Area and Data

A. Study Area

Three experimental regions in China are selected in this study (see Fig. 1): the eastern part of the Yunnan-Guizhou Plateau (YGP), the border of Shanxi Province and Henan Province (BSH), and the central part of Inner Mongolia (CIM). These regions pertain to different climatic zones and are characterized by different types of land cover and topography. Thus, the study areas are suitable for verifying the performance of the proposed downscaling method in different environmental conditions.

The YGP region is in the range of latitude 26.8°–28.7°N and longitude 108°–110.7°E, which belongs to the subtropical monsoon climate with a land cover dominated by mixed forests and woody savannas. The topography is undulating and occupied mainly by hills to moderate mountains, with an average slope of 13.5°. The BSH region is in the range of latitude 34°–36°N and longitude 110.8°–113.4°E, which belongs to the temperate monsoon climate with the land cover dominated by cropland and mixed forests. The topography is moderately undulating and mainly occupied by plains and hills, with an average slope of 8.5°. The CIM region is in the range of latitude 41.3°–43°N

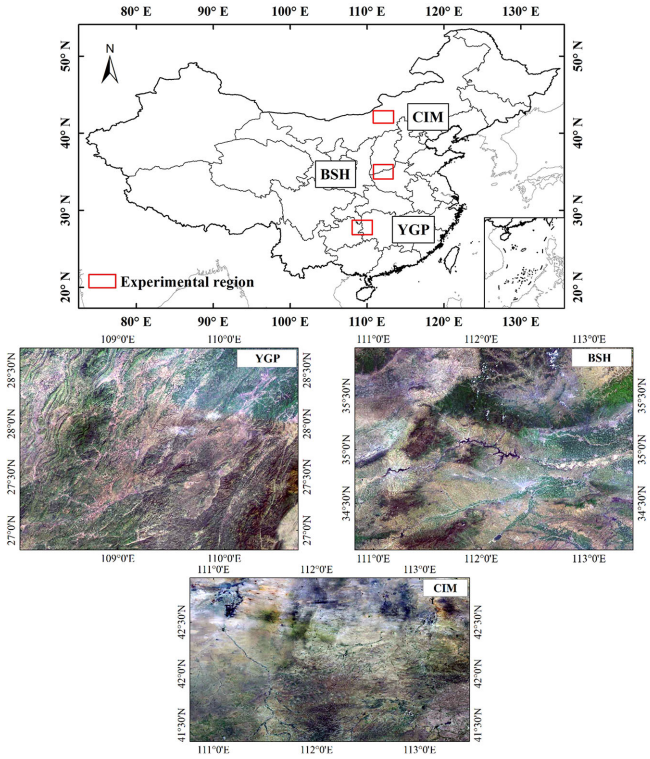

Fig. 1. Study areas. YGP, BSH, and CIM are the abbreviations for Yunnan-Guizhou Plateau, the border of Shanxi Province and Henan Province, and the central part of Inner Mongolia, respectively.

and longitude 110.8°–113.5°E, which belongs to the temperate continental climate with the land cover dominated by grassland and barren land. The topography is relatively flat and occupied mainly by plains and gentle hills, with an average slope of 2.0°.

B. Data

The datasets used for developing and assessing the MW LST downscaling method include AMSR-E LST, MODIS LST, NDVI, and shuttle radar topography mission (SRTM) elevation. Among them, the MODIS NDVI and SRTM elevation datasets serve as the scaling factors, whereas the MODIS LST dataset serves as the reference for validating the performance of the proposed method. Information describing these datasets are listed in Table I.

1) Advanced Microwave Scanning Radiometer for the Earth Observing System LAND Surface Temperature: The AMSR-E MW sensor is onboard the satellite Aqua, which functioned properly from 2002 to 2011. AMSR-E observed the Earth at approximately 1:30 A.M. and 1:30 P.M. local time. The sensor contains 12 channels centered on six frequencies (i.e., 6.9, 10.7, 18.7, 23.8, 36.5, and 89 GHz) with two polarization states (horizontal and vertical). The AMSR-E brightness temperature (BT) dataset [52] used to retrieve the LST belongs to the level 3 product (NISDC-0302) with a resolution of 0.25°. This product is derived from the level 2A product by spatial registration and resampling, in which the resolution of different frequencies ranges from 5.4 to 56 km in the reversed sequence of the frequencies mentioned above.

TABLE I
BASIC INFORMATION OF THE DATA USED IN THIS STUDY

Dataset	Spatial resolution	Coordinate systems	Time range	Temporal resolution
AMSR-E LST	0.25° (~25 km)	Equal longitude and latitude grids	2010	1/2 day
MODIS LST (MYD11A1)	1 km (~0.01°)	Sinusoidal projection	2010	1/2 day
MODIS NDVI (MYD13A2)	1 km (~0.01°)	Sinusoidal projection	2010	16 day
SRTM DEM	3″ (~90 m)	WGS 1984	-	-

Note: The datasets are originally provided in different types of coordinate systems (geographic coordinate system and projected coordinate system), so their spatial resolutions are presented in two forms for the convenience of comparison. The first values are the resolutions under the original coordinates and the values in the brackets are the transformed approximate resolutions in the other coordinate system.

The MW LST data used for developing the downscaling method were retrieved from the AMSR-E BT dataset using the algorithm proposed by Zhang and Cheng [53]. This algorithm was developed for the landmass of China considering the comprehensive effects of environmental variables, i.e., the spatiotemporal variations in land cover types, topography, and air conditions near the surface. All the 12 channels of AMSR-E data are employed to construct the empirical regression model considering the complex near-surface environment in China. Meanwhile, the stepwise regression, which automatically conducts the significance test and removes the redundant prediction terms, is adopted because the best retrieval under different environmental conditions may not always be achieved using all the 12 channels. This algorithm achieves an acceptable accuracy of LST retrieval with an RMSE in the range of 2.65–3.48 K during the daytime and 2.15–2.94 K at night in China, compared with the reference MODIS LST in the years of 2005, 2009, 2010, and 2011. This algorithm is one of the most accurate developed over China in recent years.

2) MODIS LST and NDVI: MODIS is onboard the satellites Terra and Aqua. The datasets derived from MODIS/Aqua are adopted because this sensor is on the same platform as AMSR-E. They share the same orbital geometry and transit time, so there is no need to consider the data acquisition time difference. The MODIS land surface parameters used in this study include the LST dataset (MYD11A1) [54] and the NDVI dataset (MYD13A2) [55]. MYD11A1 is the level 3 LST standard product with the resolution of 1 km, which consists of daily daytime LST, nighttime LST, and other ancillary data. The accuracy of MODIS LST is better than 1 K over homogeneous surfaces under clear sky conditions [56]. MYD13A2 is the level 3 standard product of the vegetation index with the resolution of 1 km, which provides NDVI and enhanced vegetation index every 16 days. The MODIS NDVI dataset is constructed by selecting the pixels with the lowest cloud cover, the lowest viewing angle, and the highest NDVI value within 16 days.

3) SRTM Elevation and Slope: SRTM dataset was collected by the radar onboard the space shuttle Endeavour in February 2000, which recorded the surface elevation over the continents between 60°N and 56°S, accounting for 80% of the area of the

Earth's surface. Due to its high accuracy and spatial resolution compared with contemporaneous elevation datasets, the SRTM elevation dataset has been used in many fields since its release [57], [58]. SRTM dataset has two types of spatial resolution, namely, 1"(second of arc) and 3". Zhang *et al*. [59] indicated that the bias of the 3″ SRTM elevation data in China is −0.35 m, and the 90% error (an index designed by the SRTM, i.e., the average absolute error for 90% of the area) is 7.4 m, which is better than the designed objective of 16 m. In this study, the SRTM elevation dataset at 3″ resolution is adopted due to its more extensive applications, from which the slope, which serves as a scaling factor, is also derived.

III. Methodology

A. Principle of Stepwise Downscaling

The stepwise downscaling method proposed in this study first sets a series of intermediate resolutions between the initial and the target resolutions, and downscales the LST from one resolution to the next in the series one step at a time, starting from the initial resolution and ending with the target resolution. In each step, the method applicable for TIR data that directly downscales LST from the initial resolution to the target resolution is repeatedly adopted, and the downscaled LST in the current step is treated as the one to be downscaled in the next step. In addition to the selection of scaling factor and regression model that are also involved in the direct downscaling method for TIR LST, the determination of the resolution series is a specific problem that should be focused on in stepwise downscaling.

Theoretically, the intermediate resolutions could be any number between the initial and target resolutions; however, the difference between two adjacent resolution levels in a proper resolution series should not be too large or small in order to weaken the scale effect and avoid redundant computation. According to tests of different intermediate resolution combinations including (0.05°), (0.08°, 0.03°), and (0.03°, 0.06°, 0.12°) in the three experimental regions, the series of 0.25°, 0.08°, 0.03°, and 0.01° was finally adopted taking the downscaling accuracy as the indicator. The adjacent resolution levels in this series differ from each other by about three times, which satisfies the requirement that the regression relationship is used in a relatively small scale difference.

Although various scaling factors have been introduced into different downscaling methods, in view of the complexity of environmental conditions, vegetation and topography are two fundamental factors applied in most downscaling methods. Therefore, the most widely used scaling factors NDVI, elevation, and slope are selected, considering that the stepwise process is the main concern of this study. The basic frameworks of most current TIR LST downscaling methods are the same but the regression models differ. In this study, the GWR model is used to implement the downscaling of AMSR-E LST due to its high performance when applied to TIR LST [42].

B. Geographically Weighted Regression Model

GWR is a local spatial regression method, which differs from global regression methods (e.g., least square method) in terms of the sample structure adopted by the regression model. GWR uses only the samples near the estimated point to construct the regression model, whereas global regression uses all the samples over the area of interest. Each estimated point in GWR corresponds to a unique regression model, whereas all the points in global regression share a universal regression model. Global regression assumes that the relationship between the dependent variable and independent variables is spatially constant, whereas the GWR model considers this relationship to vary in space. Because spatial heterogeneity is the natural attribute of environmental variables that leads to their relationships changing in space, the GWR model conforms to reality more closely than the global regression model. Although their applications are different, the GWR model can be regarded as an extension of the global regression model. If the global regression model is expressed as

$$y_i = \beta_0 + \sum_{k=1}^{m} \beta_k x_{ik} + \varepsilon_i \tag{1}$$

where y_i and x_{ik} are the dependent variable and the *k*th explanatory variable at location *i*, respectively; *m* is the number of explanatory variables; β_0 and β_k are the constant term and the coefficient of the *k*th explanatory variable, respectively; ε_i is the residual at location *i*, which is defined as the difference between the original values and the estimated values at the sample location and can be used to correct the error of regression model, then GWR model can be expressed as

$$y_i = \beta_0 (\mu_i, \nu_i) + \sum_{k=1}^{m} \beta_k (\mu_i, \nu_i) x_{ik} + \varepsilon_i \tag{2}$$

where μ_i and ν_i together represent the coordinate of location *i*; $\beta_0(\mu_i, \nu_i)$ and $\beta_k(\mu_i, \nu_i)$ are the constant term and the coefficient of *k*th explanatory variable at location *i*, respectively. The meanings of other parameters in (2) are the same as those in (1). The estimated point can be anywhere besides the sample locations. Under extreme conditions, when the coefficients in different locations are the same, a GWR model can be transformed into a global regression model. Despite acknowledging the spatial heterogeneity of environmental variables, GWR considers the relationship between dependent and explanatory variables to remain consistent over the local spatial extent; then the coefficients at location *i* can be regressed with the nearby samples using (1). For another location *i*+1, the coefficients can be obtained from its own nearby samples.

A critical step in GWR is to determine the size of the spatial extent in local regression. According to the First Law of Geography [60], [61], closer samples have higher contributions to the modeling of coefficients at the center location *i*, whereas the samples outside the spatial extent have no contribution. The coefficients at location *i* can therefore be derived using the least squares method integrated with weighted distance. The distance weighted least square method can be expressed as

$$\hat{\beta} (\mu_i, \nu_i) = \left(\mathbf{X}^T W (\mu_i, \nu_i) \mathbf{X}\right)^{-1} \mathbf{X}^T W (\mu_i, \nu_i) \mathbf{Y} \tag{3}$$

whereμ_i and ν_i have the same meanings with those in (1), and $\hat{\beta}(\mu_i, \nu_i)$ is the coefficient matrix at location *i* composed of $\beta_0(\mu_i, \nu_i)$ and $\beta_k(\mu_i, \nu_i)$; $\mathbf{X}$ and $\mathbf{Y}$ are the matrixes of dependent

and explanatory variables, respectively; $W(i)$ is the matrix of weighted distance that can be expressed as

$$W\ (i) = \begin{vmatrix} w_{i1} & 0 & \cdots & 0 \\ 0 & w_{i2} & \cdots & 0 \\ \vdots & \vdots & \ddots & \vdots \\ 0 & 0 & \cdots & w_{ij} \end{vmatrix} \tag{4}$$

where w_{ij} is the weight for each estimated point related to the distance between the samples and the location *i*. Several methods can be used to determine w_{ij} [62]. The one adopted in this study is

$$w_{ij} = \begin{cases} \exp\left(-d_{ij}^2/h_i^2\right), d_{ij} \le h_i \\ 0, d_{ij} > h_i \end{cases} \tag{5}$$

where d_{ij} is the distance between the sample location *j* and the estimated location *i*; h_i is the farthest distance between the samples and location *i*, and is named kernel bandwidth. There are also several methods that can be used to determine h_i [62]. The corrected Akaike information criterion ($\mathrm{AIC_c}$) with the widest applicability and good performance can be expressed as

$$\mathrm{AIC}_c = 2n\log_e(\hat{\sigma}) + n\log_e(2\pi) + n\left\{\frac{n + tr(\mathbf{S})}{n - 2 - tr(\mathbf{S})}\right\} \tag{6}$$

where *n* is the number of samples; $\hat{\sigma}$ is the estimated standard deviation of the error term; *tr*(**S**) is the trace of the hat matrix **S**, and **S** maps the model estimates $\hat{y}$ onto the sample values *y* in the following manner:

$$\hat{y} = \boldsymbol{S}y \tag{7}$$

where each row of $\boldsymbol{S}$, $\boldsymbol{r_i}$ is given by

$$\boldsymbol{r}_i = \boldsymbol{X}_i\left(\boldsymbol{X}^T W(\mu_i, \nu_i)\boldsymbol{X}\right)^{-1}\boldsymbol{X}^T W(\mu_i, \nu_i) \tag{8}$$

where h_i determines $W(\mu_i, \nu_i)$ as (5) shows; $\boldsymbol{X}_i$ is the vector of explanatory variables at each sample point. In addition, *n* and $\hat{\sigma}$ can also be obtained given h_i. Therefore, $\mathrm{AIC_c}$ is a function of h_i. The optimal h_i is determined by searching the neighborhood range of location *i* when the minimized $\mathrm{AIC_c}$ score is reached.

After getting the parameter h_i, the weighted distance matrix and further the $\hat{\beta}(\mu_i, \nu_i)$ can be obtained, then the estimated LST value at each sample location can be derived from $\beta_0(\mu_i, \nu_i)$ and $\beta_k(\mu_i, \nu_i)$ using (2). Detailed information on GWR can be found in Fotheringham *et al.* [62]. In this study, the AMSR-E LST downscaling process is achieved by the GWR tool in ArcGIS software.

C. Design of the Experiment for AMSR-E LST Downscaling

Fig. 2 shows the flow chart for the stepwise downscaling of AMSR-E LST, which can be divided into four steps.

1) Produce the scaling factors (NDVI, elevation, and slope) in the resolution series by projecting and resampling.
2) Establish the GWR model using AMSR-E LST and scaling factors starting from the initial resolution and derive the residual and coefficients at the next resolution level. At this level, the residual, used to calibrate the downscaled LST data, is derived from the residual of the sample points at the prior resolution level by kriging interpolation.

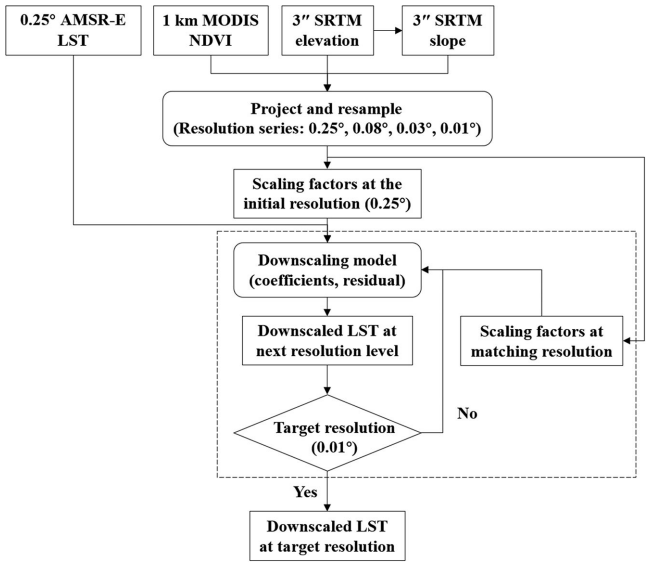

Fig. 2. Flowchart of AMSR-E LST downscaling.

3) Input the coefficients and residual derived from step 2 and the corresponding scaling factors at the same resolution into the regression model, to estimate the downscaled LST at the next resolution level.
4) Judge the next resolution level to be the target resolution or not, and if it is, end the downscaling process. Otherwise, treat the estimated LST derived from step 3 and the corresponding scaling factors as the input parameters, and repeat steps 2 and 3, to downscale the LST until the target resolution is reached.

The experiment takes the daytime data in 2010 as an example. The necessary data preprocessing includes data quality control, data filtering, data projecting and resampling, and date matching. For data quality control, the MODIS LST dataset (MYD11A1) provides a pixel-by-pixel quality control data layer for screening. Only the LST pixels marked with "good quality" and "average emissivity error < 0.02" are retained to ensure the accuracy of the regression model. For data filtering, the MODIS LST free from cloud contamination are selected because they are used to emulate all-weather AMSR-E LST by resampling in the downscaling experiment and to validate the downscaling result. Although the physical meanings of MW and TIR LSTs are different due to the thermal sampling depth (TSD, the depth that the electromagnetic wave penetrates the land surface), and the AMSR-E usually underestimates the actual LST compared with MODIS [28], [53], this emulation is feasible because the absolute accuracy of LST data is inessential in the experiment. However, completely cloud-free MODIS LST images in experimental regions are rare. To balance the spatial completeness and temporal availability of MODIS LST, the images in these three experimental regions with over 90% of the pixels available are selected. In addition, there are orbit gaps in the AMSR-E LST dataset, so the AMSR-E LST images with missing values are also excluded. Finally, the numbers of available images are 12, 32, and 33 in the YGP, BSH, and CIM regions, respectively. The

different levels of MODIS LST and NDVI, SRTM elevation and slope in the resolution series are derived by projection transformation and resampling, using the bilinear interpolation method. NDVI dataset (MYD13A2) have a temporal resolution of 16 days and are unable to match the daily MODIS LST and AMSR-E LST datasets. In this study, we assume that the variation in vegetation within 16 days can be ignored, and the NDVI from the date closest to the AMSR-E LST are therefore used as the scaling factor for downscaling. For the scaling factors of elevation and slope, we assume that the topography is invariable over the long term in the experimental regions.

Although the retrieved AMSR-E LST in this study is one of the most accurate in recent years, its accuracy is still lower than that of MODIS LST. To avoid the impact of data accuracy on the assessment of the applicability of the stepwise downscaling method, the MODIS LST is first resampled to the resolution of 0.25° to emulate the AMSR-E LST and substituted into the stepwise downscaling method. Then the downscaled LST is compared with the reference MODIS LST. Afterward, the real AMSR-E LST is applied in the stepwise downscaling method to evaluate its performance on the low-accuracy MW LST, in which the MODIS LST remains the reference. Moreover, the direct downscaling method is also included in the downscaling of AMSR-E LST for comparison.

Moran's I is an index that measures the spatial autocorrelation of environmental variables, which usually ranges between -1 and 1. When Moran's I approaches 0, the variable is randomly distributed with low spatial autocorrelation, when Moran's I gets closer to -1 or 1, the variable exhibits highly negative or positive spatial autocorrelation. Highly positive autocorrelation means that similar values are spatially aggregated, whereas highly negative autocorrelation means that nearby values are significantly of opposite sign. These two types of autocorrelation suggest a highly regular relationship among the variable values, and therefore indicate a weak spatial heterogeneity, whereas low spatial autocorrelation suggests an uncertain relationship among the randomly distributed values and indicates a high spatial heterogeneity. The spatial heterogeneity of a landscape, which could affect the performance of downscaling methods, is therefore quantified using Moran's I index of each scaling factor and their combination forms so-called total autocorrelation (TA). TA, used to indicate the general spatial heterogeneity of a landscape, is defined as

$$\mathrm{TA} = \sqrt{(M_{\mathrm{NDVI}})^2 + (M_{\mathrm{Elevation}})^2 + (M_{\mathrm{Slope}})^2} \qquad (9)$$

where M_{NDVI}, $M_{\mathrm{Elevation}}$, and M_{Slope} are Moran's I of NDVI, elevation, and slope in the experimental region, respectively. Note that a small TA value indicates strong general heterogeneity.

In the experiment of AMSR-E LST downscaling, we found that the accuracy of downscaled LST derived by the regression model involving both elevation and slope was lower than that involving only one of these two topographic parameters. Duan and Li [42] found a similar phenomenon in downscaling the TIR LST using the GWR model, i.e., the addition of unnecessary scaling factors decreased the accuracy of downscaling. Another phenomenon is that slope can achieve more accurate downscaling results in the regions with flat terrain, whereas elevation works better in the regions with steep terrain. This phenomenon is related to the spatial autocorrelation of the scaling factors [62]: Elevation over flat terrain has high autocorrelation (i.e., similar elevation values over space yield aggregation effects), leading to a poor estimate in the GWR model, as is the case for the slope in some areas with steep terrain. Therefore, the combination of both elevation and slope could not improve the accuracy of the downscaling. According to the characteristics of the landscape in the three regions, NDVI and elevation are applied in the YGP and BSH regions, whereas NDVI and slope are applied in the CIM region.

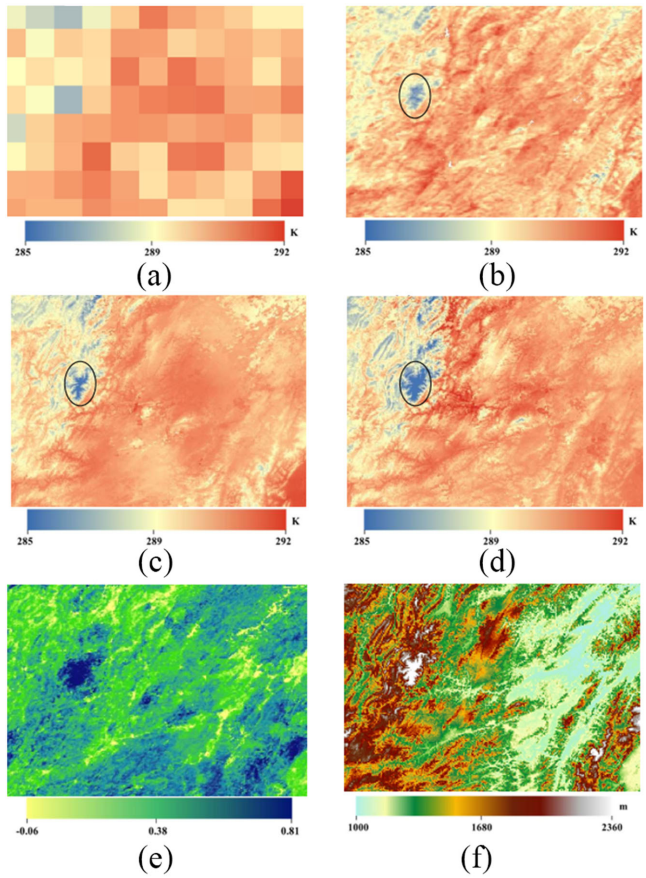

Fig. 3. Stepwise and direct downscaled LSTs from 0.25° MODIS LSTs in the YGP region. (a) 0.25° MODIS LST. (b) Original MODIS LST. (c) Stepwise downscaled LST. (d) Direct downscaled LST. (e) MODIS NDVI. (f) SRTM elevation.

IV. Results

A. Comparison Between the Stepwise and the Direct Downscaling Method Using the Emulated Data

Taking January 3 in the YGP region, November 19 in the BSH region, and October 4 in the CIM region as the examples, Figs. 3–5 show the images of the 0.25° MODIS LST (emulated AMSR-E LST), the original MODIS LST, the downscaled LST derived by the stepwise and direct methods, and the scaling factors in the

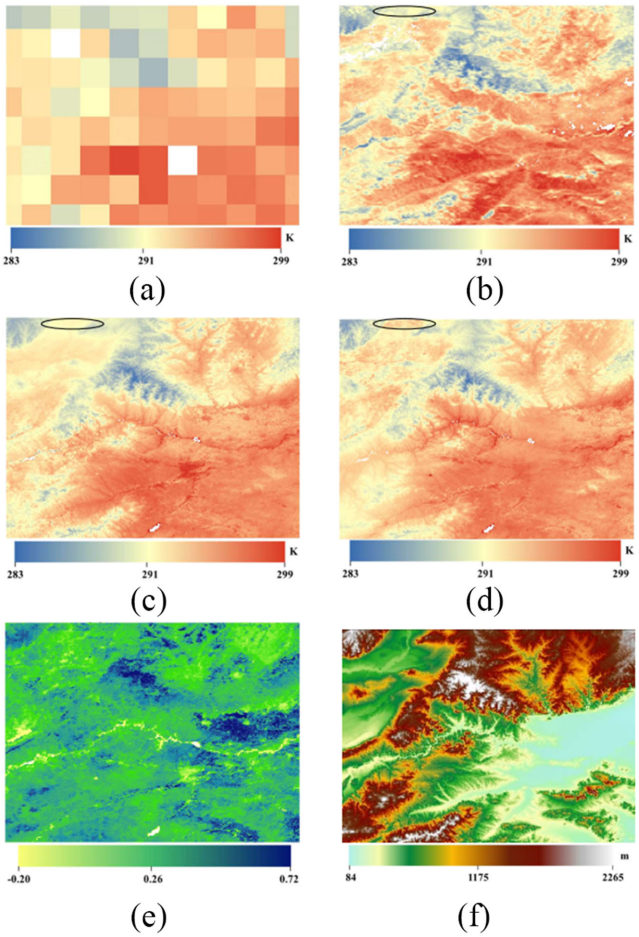

Fig. 4. Stepwise and direct downscaled LSTs from 0.25° MODIS LSTs in the BSH region. (a) 0.25° MODIS LST. (b) Original MODIS LST. (c) Stepwise downscaled LST. (d) Direct downscaled LST. (e) MODIS NDVI. (f) SRTM elevation.

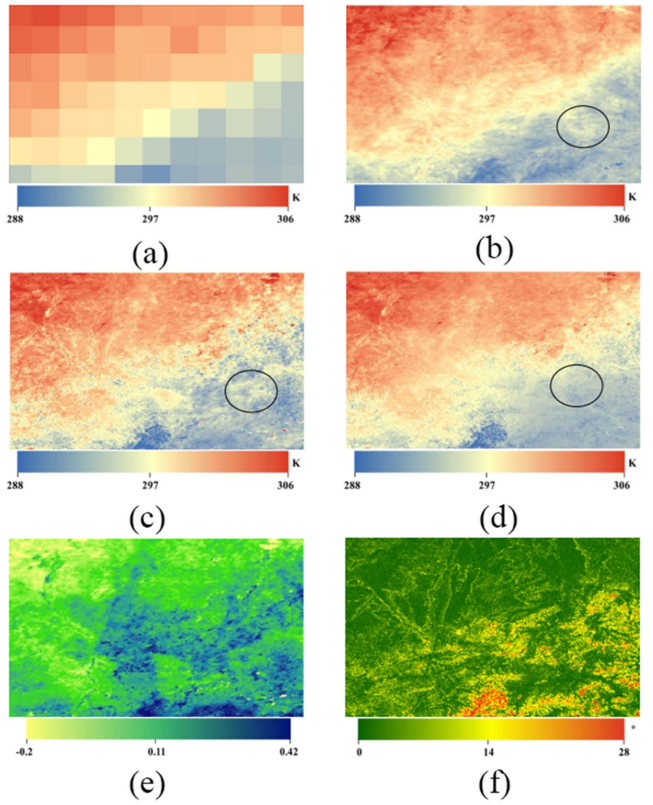

Fig. 5. Stepwise and direct downscaled LSTs from0.25° MODIS LSTs in the CIM region. (a) 0.25° MODIS LST. (b) Original MODIS LST. (c) Stepwise downscaled LST. (d) Direct downscaled LST. (e) MODIS NDVI. (f) SRTM slope.

three regions. Although a few missing values in the original MODIS LST could result in some missing values in the 0.25° MODIS LST (see Fig. 4), they do not affect the completeness of the downscaled LST because GWR can establish a regression model for any location within the extent of the samples.

From the images in the three experimental regions, the downscaled LSTs derived from the stepwise and direct methods can both reflect the general trend of LST, but the details are different. The black circles in the LST images of the three regions are the examples used to explain the differences. In the YGP and BSH regions, the spatial patterns of the downscaled LSTs from the stepwise method are more similar to the original MODIS LSTs in the black circles, whereas the direct method results in lower LST values in the YGP region and higher LST values in the BSH region. In the CIM region, although the downscaled LST derived using the stepwise method has more detailed information in terms of the spatial patterns than that derived using the direct method in the black circle, this information does not exist in the original MODIS LST. Therefore, for the black circles alone, the stepwise method performs better in the YGP and BSH regions but worse in the CIM region. In most other parts of these three regions, a similar phenomenon can be found in the downscaled LST images.

Fig. 6 shows the scatter plots between the original MODIS LST and the downscaled LST derived from the 0.25° MODIS LST using stepwise and direct methods in the three regions. The scatter data from the two downscaling methods in these three regions are generally concentrated around the 1:1 line but differ in detail. Specifically, in the YGP region, the direct method underestimates the LST in the lower range of LST compared with the stepwise method. Some part of the scatter data of these underestimated LSTs correspond to the pixels in the black circle. The RMSE of the stepwise method in this region is 0.13 K (12.9%) smaller than that of the direct method. In the BSH region, the scatter data from the stepwise method are more concentrated around the 1:1 line with an RMSE that is 0.12 K (7.0%) smaller than that of the direct method. However, the scatter plots of the two methods show some abnormalities in the upper left part, indicating that these two methods both overestimate the LST. These abnormalities mainly result from the Yellow River passing through the BSH region from west to east and some scattered urban areas in this region. NDVI and topography cannot capture the correct variation in temperature over these land cover types. In the CIM region, the scatter plot from the direct method is more concentrated around the 1:1 line with fewer outliers. The RMSE of the stepwise method in this

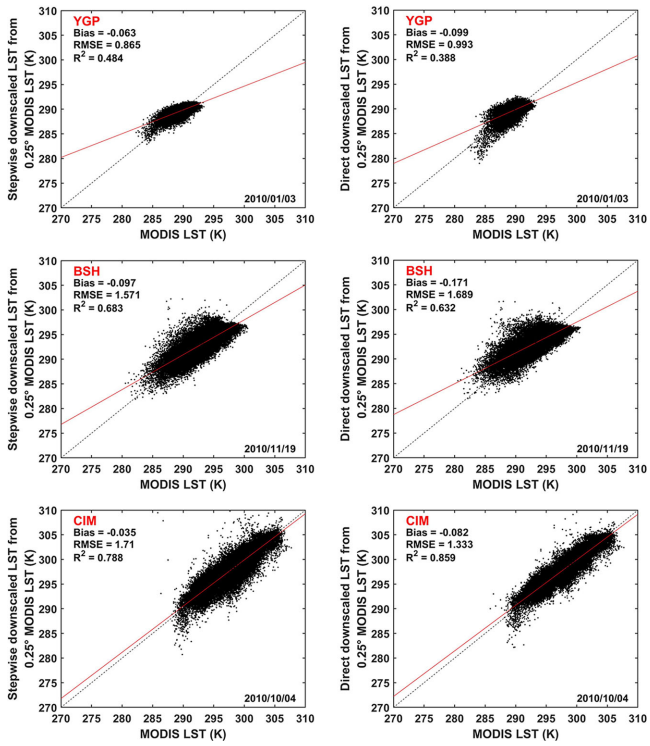

Fig. 6. Scatter plots between the original MODIS LST and the stepwise and direct downscaled LSTs from the 0.25° MODIS LST in the experimental regions. The black dash line is the 1:1 line, while the red line is the linear regression line of the scatter data.

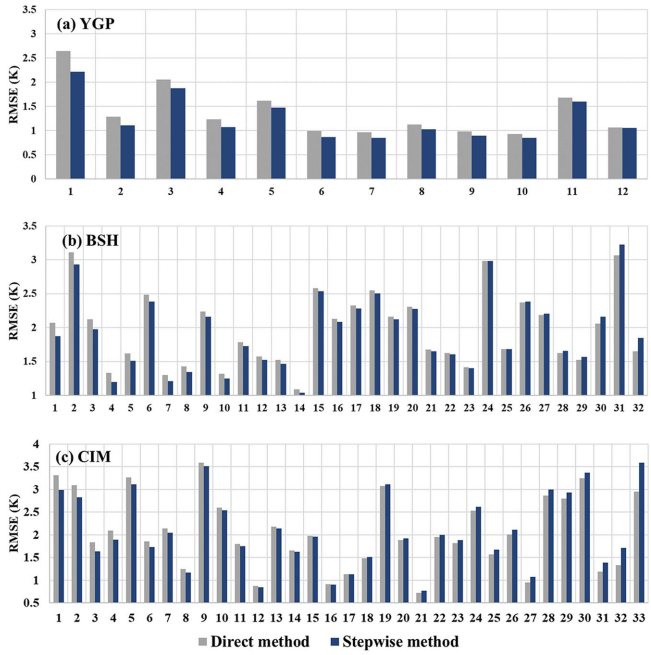

Fig. 7. RMSE between the original MODIS LST and the downscaled LST from the stepwise and direct downscaling methods in the three regions. The *x*-axis indicates the number of images on different dates, and the dates are sorted in a decreasing manner according to the difference of RMSE between the direct and the stepwise downscaled LSTs.

region is 0.38 K (28.5%) larger than that of the direct method. The R^2 of the scatter data increases in the sequence of YGP, BSH, and CIM for both downscaling methods, and the R^2 of the stepwise method is higher than that of the direct method in the YGP and BSH regions, but smaller than that of the direct method in the CIM region. The liner regression line (red) of the downscaled LST versus MODIS LST shows different slopes, in which the slope for the regression line in the CIM region is much closer to the 1:1 line whereas the slope for the regression line in the YGP region is much more distant from the 1:1 line.

To explore a more general relationship between the stepwise and the direct downscaling results, the RMSEs between the original MODIS LST and the downscaled 0.25° MODIS LSTs from these two methods on the available dates for the three regions are shown in Fig. 7. The dates are sorted in a decreasing manner according to the RMSE difference between the direct and the stepwise downscaled LSTs. In the YGP region, the RMSEs of the stepwise downscaled LST on all dates are smaller than those of the direct downscaled LST, which means that the stepwise method can achieve better downscaling results in the regions similar to the YGP. The mean difference of the RMSE between the two methods is 0.14 K, meaning the stepwise method improved the accuracy by 10.3% on average. In the BSH region, the RMSEs of the stepwise downscaled LST are smaller than those of the direct downscaled LST for 25 days, accounting for 78.1% of the available dates. This result confirms that the stepwise method can achieve better results with high probability in the regions similar to the BSH. On the days when the stepwise method is better, the mean difference of the RMSE between two methods is 0.07 K, meaning the stepwise method improved the accuracy by 3.5% on average; whereas on the days when the direct method is better, the mean difference of the RMSE between the two methods is 0.08 K, meaning the direct method achieves higher accuracy by 3.5% on average. In the CIM region, the RMSEs of the stepwise downscaled LST are smaller than those of the direct downscaled LST for 17 days, accounting for 51.5% of the available dates. This means that the stepwise and direct methods can achieve better downscaled results with similar probability in regions like the CIM. On the days that the stepwise method is better, the mean difference of the RMSE between the two methods is 0.11 K, meaning the stepwise method improved the accuracy by 4.7% on average; whereas on the days that the direct method is better, the mean difference of the RMSE between the two methods is 0.14 K, meaning the direct method achieved higher accuracy by 7.0% on average.

B. *Downscaling of the Real AMSR-E LST*

Fig. 8 shows the images of downscaled LST derived from the real AMSR-E LST in the three regions. The dates for these images are the same as those in Section IV-A. According to the performance of the two downscaling methods in the landscapes with different characteristics, the stepwise method is applied in the YGP and BSH regions, whereas the direct method is applied in the CIM region. The scaling factors for the real AMSR-E LST in each region are also consistent with those in Section IV-A.

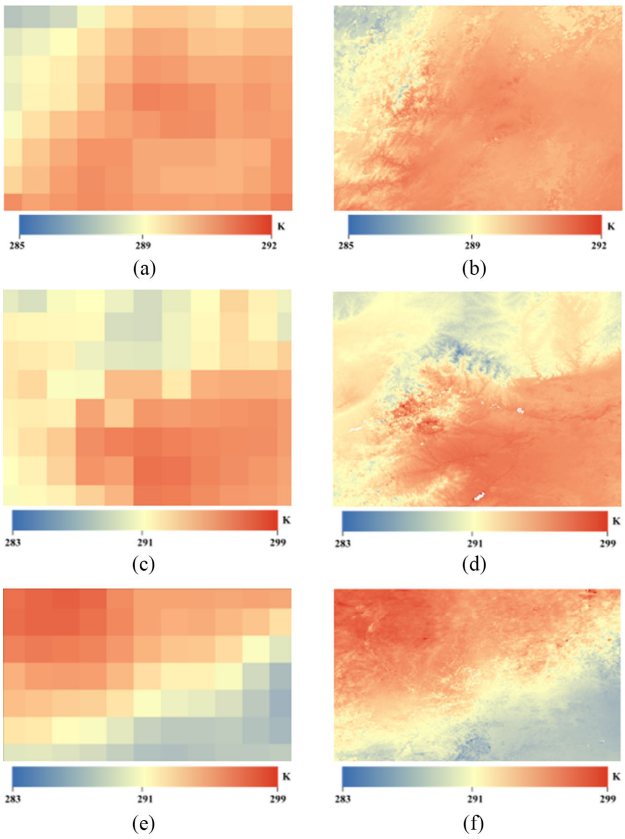

Fig. 8. Downscaled LST from the real AMSR-E LST in the three regions. (a) Real AMSR-E LST in the YGP region. (b) Stepwise downscaled LST in the YGP region. (c) Real AMSR-E LST in the BSH region. (d) Stepwise downscaled LST in the BSH region. (e) Real AMSR-E LST in the CIM region. (f) Direct downscaled LST in the CIM region.

From the spatial patterns, although the general spatial trend of the downscaled LST from the real AMSR-E LST (see Fig. 8) is similar to that from the 0.25° MODIS LST (see Figs. 3–5), some of the detailed information in the LST image is missing in each region, especially in the YGP and BSH regions. In the YGP region, the downscaled LST from the real AMSR-E LST shows the correct trend, i.e., the LST values in the eastern part are higher than those in the west part; however, the more localized high values in the western part and the local low values in the eastern part have been lost. A similar phenomenon appears in the BSH region as well, although more detailed information is presented. For example, in the northern and western parts of the BSH region, the downscaled LST from the real AMSR-E LST has weakened the contrast of the LST pattern. In the CIM region, the downscaled LST from the real AMSR-E LST is very similar to that from the 0.25° MODIS LST. Both reflect the trend and detailed information that the LST decreases from the northwestern part to the southeastern part. The correlation coefficients between the downscaled LSTs from the 0.25° MODIS LST and the real AMSR-E LST are 0.74, 0.93, and 0.96 in the YGP, BSH, and CIM regions, respectively, indicating that the similarity of the downscaled LSTs from two types of AMSR-E LST datasets is relatively small in the YGP region, relatively large in the CIM region, and moderate in the BSH region.

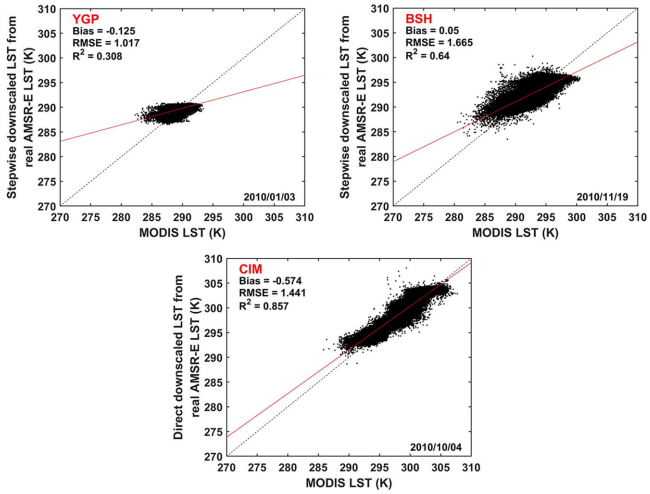

Fig. 9. Scatter plots between the reference MODIS LST and the downscaled LST from the real AMSR-E LST in the three regions. The black dash line is the 1:1 line, while the red line is the linear regression line of the scatter data.

Further comparisons reveal that the performance of downscaling methods is related to the quality of the original AMSR-E LST. From the spatial patterns, the 0.25° MODIS LSTs in the three regions possess more detailed information, and the downscaled LSTs inherit these features (see Figs. 3–5). In contrast, the real AMSR-E LSTs in the three regions are relatively smooth in the pattern, leading to less information in the downscaled LST (see Fig. 8). The correlation coefficients between the 0.25° MODIS LST and the real AMSR-E LST are 0.62, 0.88, and 0.97 in the YGP, BSH, and CIM regions, respectively. This order is consistent with that of the downscaled LST derived from these two types of AMSR-E LST datasets. That is, the downscaled LST inherits the spatial pattern of the original AMSR-E LST before downscaling.

Fig. 9 shows the scatter plots between the reference MODIS LST and the downscaled LST from real AMSR-E LST in the three regions. The value range of the downscaled LST in each region is narrowed to a certain extent compared with the reference MODIS LST values, especially in the YGP and BSH regions. In addition, synthesizing the information from Figs. 6 and 9, the RMSE between the reference MODIS LST and the downscaled real AMSR-E LST in the three regions has increased to different extents compared with the RMSE from the 0.25° MODIS LST, using the same downscaling methods. This result verifies that the accuracy of downscaled LST from the real LST dataset generally cannot reach that from the 0.25° MODIS LST. The R^2 and the slope of the regression line of real AMSR-E LST show a similar trend with that of 0.25° MODIS LST.

V. Discussion

The performance of the stepwise downscaling method is assessed using the 0.25° MODIS LST (emulated AMSR-E LST) in three experimental regions that represent different characteristics of topography and vegetation. Table II shows the Moran's I of each scaling factor and TA in the three regions. Both the

TABLE II
MORAN'S I OF THE SCALING FACTORS AND THE TA IN EACH EXPERIMENTAL REGION

Region	NDVI	Elevation	Slope	TA
YGP	0.49	0.77	0.27	0.95
BSH	0.74	0.94	0.65	1.35
CIM	0.80	0.99	0.52	1.37

Note: Moran's I values of NDVI, elevation, and slope in the three regions pass the significance testing with a *P*-value of 0.

TABLE III
OPTIMAL BANDWIDTH FOR EACH STEP OF DOWNSCALING IN THE THREE REGIONS IN THE EXAMPLE DATES

Region	Step 1 (0.25°-0.08°)	Step 2 (0.08°-0.03°)	Step 3 (0.03°-0.01°)
YGP	77.25	37.76	23.82
BSH	88.08	45.58	26.33
CIM	96.70	55.09	39.44

Note: The unit of bandwidth h_i value is km.

NDVI and elevation of these regions show increasing trends in the order of YGP, BSH, and CIM, which means the spatial heterogeneity of these two scaling factors is strongest in the YGP region, moderate in the BSH region, and weakest in the CIM region. The trend of slope is not straightforward, which is reflected in the fact that the weakest heterogeneity is in the BSH region where the topography is moderately undulating, but not in the CIM region where the topography is relatively flat. The reason for this finding is the slope over some steeper terrains has an aggregation effect due to the long straight slope surface, but the slope over plains may be disordered due to the up-and-down land covers, even if the slopes have similar values. Nevertheless, the general heterogeneity is still strongest in the YGP region and weakest in the CIM region.

The GWR model selects the nearby sample points with a strong correlation to establish the local regression relationship; therefore, the optimal bandwidth h_i in (5) is small when the spatial heterogeneity of environmental variables is strong, whereas the optimal h_i is large when the spatial heterogeneity of environmental variables is weak. The optimal h_i for each step of downscaling in the three regions in the example dates have been extracted. The statistics of h_i are list in Table III.

For each step, the optimal h_i increases as the spatial heterogeneity of region gets weaker. For each region, the optimal h_i decreases as the resolution gets higher. The relationship between h_i and resolution actually related to the heterogeneity as well. The coarse resolution of LST and scaling factors data smooth the variation of environmental variables, leading to an underestimation of the spatial heterogeneity of a region. Therefore, the statistics of h_i in these cases conform to the mechanism of GWR very well.

The verification results show that the stepwise method is more advantageous in downscaling the AMSR-E LST in the region with strong spatial heterogeneity than is the direct method. This advantage is weakened when the vegetation becomes sparser and more uniform and the terrain becomes flatter, namely, in more spatially homogeneous areas. The scale effect is strong in regions with high heterogeneity, but weak in regions with low heterogeneity. The capability of the stepwise method to weaken the scale effect is prominent when the spatial heterogeneity is high. This capability is due to the multiple residual corrections made during the stepwise downscaling process. Although the stepwise method is better than the direct method in the regions with high heterogeneity, the goodness of fit of the two downscaling methods is higher in the regions with low heterogeneity, as reflected in the R^2 and slope of the regression line.

The initial and target resolutions in the stepwise method are identical to those in the direct method, but the former includes more scaling processes. Hence, the scale differences among these processes during stepwise downscaling are smaller than those before and after the direct downscaling process. The uncertainty in the introduction of resolution series in the stepwise downscaling process is mainly caused by error propagation when constructing the regression relationship from the GWR model estimated LST; however, this uncertainty could be corrected by introducing the residual term. The residual correction in each step of the stepwise downscaling process greatly weakens the error propagation. Although the residual term is also included in the direct downscaling method, its accuracy cannot compete with that in each step of the stepwise downscaling process. In the direct downscaling process, the residual term obtained by spatial interpolation directly from the initial resolution to the target resolution has lower accuracy due to the large scale differences between these two resolutions. In the stepwise downscaling process, however, the scale difference between the two adjacent resolution levels is relatively small, so the residual term at each resolution level obtained by the spatial interpolation is more accurate. By applying the GWR model without residual correction, the advantage of the stepwise method compared to the direct method is weakened to different extents in the three regions. The proportion of dates when the stepwise method was better decreased by 58.3%, 15.6%, and 12.1% in the YGP, BSH, and CIM regions, respectively. This result indicates that the multiple residual correction is the key reason why the stepwise method is better than the direct method and multiple residual correction can improve the accuracy of the downscaled LST more efficiently in the regions with high heterogeneity. When the spatial heterogeneity is weak, the small scale difference leads to the accuracy of the interpolated residual term in the direct method being comparable to that in the stepwise mothed, so there is little difference between the stepwise method and the direct method in downscaling the AMSR-E LST.

The comparison of the downscaling process between the 0.25° MODIS LST and real AMSR-E LSTs indicates that the spatial patterns of the downscaled LST inherits the patterns before downscaling, and the accuracy of the downscaled LST from real LST dataset generally cannot reach the accuracy of the 0.25° MODIS LST. Other studies on LST downscaling found similar phenomena: the downscaled LST from real LST exhibited smooth spatial patterns, whereas the downscaled LST

from 0.25° MODIS LST was more realistic [44], [63]. Compared with the 0.25° MODIS LST, the real AMSR-E LST usually has relatively low accuracy due to low resolution, penetration depth, and complex emission mechanisms of MW and the limitations of MW LST retrieval algorithm. Nevertheless, the detailed information of the spatial variation of the downscaled LST derived from the real AMSR-E LST is still much richer than that before downscaling and is generally similar to the reference MODIS LST in patterns.

VI. Conclusion

In this study, a stepwise downscaling method is developed for generating high-resolution LST from an AMSR-E dataset to promote the fusion of TIR and MW LSTs. This method is based on the GWR model, in which NDVI, elevation, and slope are selected as the scaling factors. In the three regions that represent different landscape characteristics, the stepwise method is compared to the traditional direct downscaling method that was originally designed for TIR LST.

During the assessment of the applicability of stepwise method using the emulated AMSR-E LST (0.25° MODIS LST) data, although the downscaling results derived from the stepwise and direct methods could both reflect the correct LST spatial patterns, the results of the former method were generally closer to the reference MODIS LST in detail, especially in the regions with high heterogeneity. On the example days, the RMSEs of the stepwise method were 0.13 K (12.9%) and 0.12 K (7.0%) smaller than those of the direct method in the YGP and BSH regions. On the available days in 2010, the proportion of dates when the stepwise method was better than the direct method was 100%, 78.1%, and 51.5% in the YGP, BSH, and CIM regions, respectively. The advantage of the stepwise method is closely related to the heterogeneity of the landscape. The scale effect is significant in the region with high heterogeneity, but weak in the region with low heterogeneity. The stepwise method can reduce the impact of scale effect on the downscaling result to some extent, and its advantage is prominent when the scale effect is significant. The mechanism for this advantage is that the stepwise method contains multiple residual correction processes.

The experiment on real AMSR-LST downscaling indicates that accurate AMSR-E LST guarantees better downscaling results because the downscaled LST inherits the spatial patterns of the original AMSR-E LST before downscaling. The real AMSR-E LST, which usually exhibits a smoother pattern and lower accuracy, inevitably results in lower contrast and accuracy of the downscaled LST, as shown in the YGP and BSH regions. Due to the importance of accurate original MW LST in spatial downscaling, as done by many studies on LST downscaling, including this study, the verification of the downscaling method always starts with emulated LST. Although the AMSR-E LST retrieval algorithm has been improved greatly in recent years, the accuracy of the retrieved LST still cannot reach that of TIR LST over most landscapes. Nevertheless, the downscaling process has enriched the detailed information in the real AMSR-E LST dataset.

Using 0.25° MODIS LST, the stepwise downscaling method especially proposed for MW LST performed better compared with the traditional direct downscaling method, especially in the relatively heterogeneous regions. The downscaled LST from real AMSR-E LST using the stepwise method was also more beneficial to the fusion of AMSR-E and MODIS LSTs than the direct method used in the previous studies.

The selection of scaling factors is one of the key elements affecting the quality of the LST downscaling model. In this study, only the commonly used parameters NDVI, elevation, and slope were adopted because the major concern is the stepwise process in AMSR-E LST downscaling. This restriction leads to some errors in the downscaling results over land cover types such as water and urban areas. According to the studies of scaling factors in TIR LST downscaling, it is expected that the addition of other scaling factors related to the variation of LST could further improve the accuracy of the stepwise downscaling method. The stepwise downscaling method proposed in this study is based on the GWR model; however, a number of other regression models have been used to develop the TIR LST downscaling methods. Theoretically, these models could be incorporated into the MW LST stepwise downscaling method as well. The determination of intermediate resolution series, a new parameter in stepwise downscaling process compared with the direct downscaling method, should also be considered when facing different MW LST datasets. Further research is expected to obtain more accurate downscaled MW LST by improving the stepwise downscaling method, so as to enhance the quality of MW and TIR LST data fusion and benefit the application of LST products in remote sensing community.

References

[1] M. Anderson, J. Norman, W. Kustas, R. Houborg, P. Starks, and N. Agam, "A thermal-based remote sensing technique for routine mapping of land-surface carbon, water and energy fluxes from field to regional scales," *Remote Sens. Environ.*, vol. 112, no. 12, pp. 4227–4241, 2008.

[2] J. Cheng and W. P. Kustas, "Using very high resolution thermal infrared imagery for more accurate determination of the impact of land cover differences on evapotranspiration in an irrigated agricultural area," *Remote Sens.*, vol. 11, no. 6, Mar. 2019, Art. no. 613.

[3] J. D. Kalma, T. R. McVicar, and M. F. McCabe, "Estimating land surface evaporation: A review of methods using remotely sensed surface temperature data," *Surveys Geophys.*, vol. 29, no. 4–5, pp. 421–469, 2008.

[4] Z.-L. Li *et al.*, "A review of current methodologies for regional evapotranspiration estimation from remotely sensed data," *Sensors*, vol. 9, no. 5, pp. 3801–3853, 2009.

[5] K. Trenberth *et al.*, "Observations: Surface and atmospheric climate change," in *Climate Change*, 2007, ch. 3, pp. 235–336.

[6] J. Zhou, Y. Chen, J. Wang, and W. Zhan, "Maximum nighttime urban heat island (UHI) intensity simulation by integrating remotely sensed data and meteorological observations," *IEEE J. Sel. Topics Appl. Earth Observ. Remote Sens.*, vol. 4, no. 1, pp. 138–146, Mar. 2011.

[7] Y. Zhang and J. Cheng, "Spatio-temporal analysis of urban heat island using multisource remote sensing data: A case study in Hangzhou, China," *IEEE J. Sel. Topics Appl. Earth Observ. Remote Sens.*, vol. 12, no. 9, pp. 3317–3326, Sep. 2019.

[8] Z. Li *et al.*, "Satellite-derived land surface temperature: Current status and perspectives," *Remote Sens. Environ.*, vol. 131, pp. 14–37, 2013.

[9] H. Ma, S. Liang, Z. Xiao, and D. Wang, "Simultaneous estimation of multiple land-surface parameters from VIIRS optical-thermal data," *IEEE Geosci. Remote Sensing Letters*, vol. 15, no. 1, pp. 156–160, Jan. 2018.

[10] H. Ma *et al.*, "Simultaneous inversion of multiple land surface parameters from MODIS optical–thermal observations," *ISPRS J. Photogrammetry Remote Sensing*, vol. 128, pp. 240–254, 2017.

[11] M. Jin, "Interpolation of surface radiative temperature measured from polar orbiting satellites to a diurnal cycle: 2. Cloudy–pixel treatment," *J. Geophys. Res., Atmos.*, vol. 105, no. D3, pp. 4061–4076, 2000.

[12] Z. Shao, Y. Pan, C. Diao, and J. Cai, "Cloud detection in remote sensing images based on multiscale feature-convolutional neural network," *IEEE Trans. Geosci. Remote Sens.*, vol. 57, no. 6, pp. 4062–4076, Jun. 2019.

[13] C. Huang *et al.*, "Intercomparison of AMSR2-and MODIS-derived land surface temperature under clear-sky conditions," *IEEE J. Sel. Topics Appl. Earth Observ. Remote Sens.*, vol. 12, no. 9, pp. 3286–3294, Sep. 2019.

[14] T. I. Østby, T. V. Schuler, and S. Westermann, "Severe cloud contamination of MODIS land surface temperatures over an Arctic ice cap, Svalbard," *Remote Sens. Environ.*, vol. 142, no. Supplement C, pp. 95–102, 2014.

[15] Q. Weng, P. Fu, and F. Gao, "Generating daily land surface temperature at Landsat resolution by fusing Landsat and MODIS data," *Remote Sens. Environ.*, vol. 145, no. Supplement C, pp. 55–67, 2014.

[16] T. Wang, J. Shi, G. Yan, T. Zhao, D. Ji, and C. Xiong, "Recovering land surface temperature under cloudy skies for potentially deriving surface emitted longwave radiation by fusing MODIS and AMSR-E measurements," in *Proc. IEEE Int. Geosci. Remote Sens. Symp.*, 2014, pp. 1805–1808.

[17] X. Kou, L. Jiang, Y. Bo, S. Yan, and L. Chai, "Estimation of land surface temperature through blending MODIS and AMSR-E data with the Bayesian maximum entropy method," *Remote Sens.*, vol. 8, no. 2, 2016, Art. no. 105.

[18] S.-B. Duan, Z.-L. Li, and P. Leng, "A framework for the retrieval of all-weather land surface temperature at a high spatial resolution from polar-orbiting thermal infrared and passive microwave data," *Remote Sens. Environ.*, vol. 195, pp. 107–117, 2017.

[19] D. Sun *et al.*, "Land surface temperature derivation under all sky conditions through integrating AMSR-E/AMSR-2 and MODIS/GOES observations," *Remote Sens.*, vol. 11, no. 14, 2019, Art. no. 1704.

[20] X. Zhang, J. Zhou, F.-M. Göttsche, W. Zhan, S. Liu, and R. Cao, "A method based on temporal component decomposition for estimating 1-km all-weather land surface temperature by merging satellite thermal infrared and passive microwave observations," *IEEE Trans. Geosci. Remote Sens.*, vol. 57, no. 7, pp. 4670–4691, Jul. 2019.

[21] S. Xu, J. Cheng, and Q. Zhang, "Reconstructing all-weather land surface temperature using the Bayesian maximum entropy method over the tibetan plateau and heihe river basin," *IEEE J. Sel. Topics Appl. Earth Observ. Remote Sens.*, vol. 12, no. 9, pp. 3307–3316, Sep. 2019.

[22] C. Huang *et al.*, "A physically based algorithm for retrieving land surface temperature under cloudy conditions from AMSR2 passive microwave measurements," *Int. J. Remote Sens.*, vol. 40, no. 5–6, pp. 1828–1843, 2018.

[23] M. J. McFarland, R. L. Miller, and C. M. Neale, "Land surface temperature derived from the SSM/I passive microwave brightness temperatures," *IEEE Trans. Geosci. Remote Sens.*, vol. 28, no. 5, pp. 839–845, Sep. 1990.

[24] T. R. H. Holmes, R. A. M. De Jeu, M. Owe, and A. J. Dolman, "Land surface temperature from Ka band (37 GHz) passive microwave observations," *J. Geophys. Res., Atmos.*, vol. 114, no. D4, 2009, Art. no. D04113.

[25] K. Mao, J. Shi, Z. Li, Z. Qin, M. Li, and B. Xu, "A physics-based statistical algorithm for retrieving land surface temperature from AMSR-E passive microwave data," *Sci. China Series D, Earth Sci.*, vol. 50, no. 7, pp. 1115–1120, 2007.

[26] M. Owe and A. A. Van De Griend, "On the relationship between thermodynamic surface temperature and high-frequency (37 GHz) vertically polarized brightness temperature under semi-arid conditions," *Int. J. Remote Sens.*, vol. 22, no. 17, pp. 3521–3532, 2001.

[27] J. Hollinger, *DMSP Special Sensor Microwave/Imager Calibration/Validation*. Washington DC, USA: Naval Res. Lab, 1991.

[28] J. Zhou, F. Dai, X. Zhang, S. Zhao, and M. Li, "Developing a temporally land cover-based look-up table (TL-LUT) method for estimating land surface temperature based on AMSR-E data over the Chinese landmass," *Int. J. Appl. Earth Observ. Geoinf.*, vol. 34, pp. 35–50, 2015.

[29] F.-C. Zhou, Z.-L. Li, H. Wu, S.-B. Duan, X. Song, and G. Yan, "A practical two-stage algorithm for retrieving land surface temperature from AMSR-E data—A case study over China," *IEEE J. Sel. Topics Appl. Earth Observ. Remote Sens.*, vol. 11, no. 6, pp. 1939–1948, Jun. 2018.

[30] W. Zhan *et al.*, "Disaggregation of remotely sensed land surface temperature: Literature survey, taxonomy, issues, and caveats," *Remote Sens. Environ.*, vol. 131, pp. 119–139, 2013.

[31] M. Stathopoulou and C. Cartalis, "Downscaling AVHRR land surface temperatures for improved surface urban heat island intensity estimation," *Remote Sens. Environ.*, vol. 113, no. 12, pp. 2592–2605, 2009.

[32] C. Jeganathan, N. Hamm, S. Mukherjee, P. M. Atkinson, P. Raju, and V. Dadhwal, "Evaluating a thermal image sharpening model over a mixed agricultural landscape in India," *Int. J. Appl. Earth Observ. Geoinf.*, vol. 13, no. 2, pp. 178–191, 2011.

[33] W. P. Kustas, J. M. Norman, M. C. Anderson, and A. N. French, "Estimating subpixel surface temperatures and energy fluxes from the vegetation index–radiometric temperature relationship," *Remote Sens. Environ.*, vol. 85, no. 4, pp. 429–440, 2003.

[34] N. Agam, W. P. Kustas, M. C. Anderson, F. Li, and C. M. Neale, "A vegetation index based technique for spatial sharpening of thermal imagery," *Remote Sens. Environ.*, vol. 107, no. 4, pp. 545–558, 2007.

[35] W. Essa, B. Verbeiren, J. van der Kwast, and O. Batelaan, "Improved DisTrad for downscaling thermal MODIS imagery over urban areas," *Remote Sens.*, vol. 9, no. 12, p. 1243, 2017.

[36] K. Zakšek and K. Oštir, "Downscaling land surface temperature for urban heat island diurnal cycle analysis," *Remote Sens. Environ.*, vol. 117, pp. 114–124, 2012.

[37] W. Essa, J. van der Kwast, B. Verbeiren, and O. Batelaan, "Downscaling of thermal images over urban areas using the land surface temperature–impervious percentage relationship," *Int. J. Appl. Earth Observ. Geoinf.*, vol. 23, pp. 95–108, 2013.

[38] Y. Yang, X. Li, X. Pan, Y. Zhang, and C. Cao, "Downscaling land surface temperature in complex regions by using multiple scale factors with adaptive thresholds," *Sensors*, vol. 17, no. 4, 2017, Art. no. 744.

[39] J. Nichol, "An emissivity modulation method for spatial enhancement of thermal satellite images in urban heat island analysis," *Photogramm. Eng. Remote Sens.*, vol. 75, no. 5, pp. 547–556, 2009.

[40] A. Dominguez, J. Kleissl, J. C. Luvall, and D. L. Rickman, "High-resolution urban thermal sharpener (HUTS)," *Remote Sens. Environ.*, vol. 115, no. 7, pp. 1772–1780, 2011.

[41] G. Yang, R. Pu, C. Zhao, W. Huang, and J. Wang, "Estimation of subpixel land surface temperature using an endmember index based technique: A case examination on ASTER and MODIS temperature products over a heterogeneous area," *Remote Sens. Environ.*, vol. 115, no. 5, pp. 1202–1219, 2011.

[42] S.-B. Duan and Z.-L. Li, "Spatial downscaling of MODIS land surface temperatures using geographically weighted regression: Case study in northern China," *IEEE Trans. Geosci. Remote Sens.*, vol. 54, no. 11, pp. 6458–6469, Nov. 2016.

[43] P. Sismanidis, I. Keramitsoglou, B. Bechtel, and C. T. Kiranoudis, "Improving the downscaling of diurnal land surface temperatures using the annual cycle parameters as disaggregation kernels," *Remote Sens.*, vol. 9, no. 1, 2016, Art. no. 23.

[44] C. Hutengs and M. Vohland, "Downscaling land surface temperatures at regional scales with random forest regression," *Remote Sens. Environ.*, vol. 178, no. Supplement C, pp. 127–141, 2016.

[45] L. Jing and Q. Cheng, "A technique based on non-linear transform and multivariate analysis to merge thermal infrared data and higher-resolution multispectral data," *Int. J. Remote Sens.*, vol. 31, no. 24, pp. 6459–6471, 2010.

[46] E. Pardo-Igúzquiza, M. Chica-Olmo, and P. M. Atkinson, "Downscaling cokriging for image sharpening," *Remote Sens. Environ.*, vol. 102, no. 1–2, pp. 86–98, 2006.

[47] V. Rodriguez-Galiano, E. Pardo-Igúzquiza, M. Sanchez-Castillo, M. Chica-Olmo, and M. Chica-Rivas, "Downscaling Landsat 7 ETM+ thermal imagery using land surface temperature and NDVI images," *Int. J. Appl. Earth Observ. Geoinf.*, vol. 18, pp. 515–527, 2012.

[48] G. Yang, R. Pu, W. Huang, J. Wang, and C. Zhao, "A novel method to estimate subpixel temperature by fusing solar-reflective and thermal-infrared remote-sensing data with an artificial neural network," *IEEE Trans. Geosci. Remote Sens.*, vol. 48, no. 4, pp. 2170–2178, Apr. 2010.

[49] V. M. Bindhu, B. Narasimhan, and K. P. Sudheer, "Development and verification of a non-linear disaggregation method (NL-DisTrad) to downscale MODIS land surface temperature to the spatial scale of Landsat thermal data to estimate evapotranspiration," *Remote Sens. Environ.*, vol. 135, no. 8, pp. 118–129, 2013.

[50] P. Yao, J. Shi, T. Zhao, M. H. Cosh, R. Bindlish, and H. Lu, "An l-band brightness temperature disaggregation method using s-band radiometer data for the water cycle observation mission (WCOM)," *IEEE J. Sel. Topics Appl. Earth Observ. Remote Sens.*, vol. 12, no. 9, pp. 3184–3193, Sep. 2019.

[51] N. Ye *et al.*, "Evaluation of SMAP downscaled brightness temperature using SMAPEx-4/5 airborne observations," *Remote Sens. Environ.*, vol. 221, pp. 363–372, Feb. 2019.

[52] K. Knowles, M. Savoie, R. Armstrong, and M. J. Brodzik, *AMSR-E/Aqua Daily Global Quarter-Degree Gridded Brightness Temperatures*, Version 1. Boulder, Colorado, USA: NASA National Snow and Ice Data Center Distributed Active Archive Center, 2006, doi: 10.5067/RRR4WWORG070.

[53] Q. Zhang and J. Cheng, "An empirical algorithm for retrieving land surface temperature from AMSR-E data considering the comprehensive effects of environmental variables," *Earth Space Sci.*, vol. 7, 2020, Art. no. e2019EA001006.
[54] Z. Wan, S. Hook, and G. Hulley, "MYD11A1 MODIS/aqua land surface temperature and the emissivity daily L3 global 1km SIN grid," NASA LP DAAC, 2015, doi: 10.5067/MODIS/MYD11A1.006.
[55] K. Didan and A. Huete, "MYD13A2 MODIS/aqua vegetation indices 16-Day L3 global 1km SIN grid," NASA LP DAAC, 2015, doi: 10.5067/MODIS/MYD13A2.006.
[56] Z. Wan, "New refinements and validation of the MODIS land-surface temperature/emissivity products," *Remote Sens. Environ.*, vol. 112, no. 1, pp. 59–74, 2008.
[57] L. Yang, X. Meng, and X. Zhang, "SRTM DEM and its application advances," *Int. J. Remote Sens.*, vol. 32, no. 14, pp. 3875–3896, 2011.
[58] P. Zandbergen, "Applications of shuttle radar topography mission elevation data," *Geography Compass*, vol. 2, no. 5, pp. 1404–1431, 2008.
[59] Q. Zhang, Q. Yang, and C. Wang, "SRTM error distribution and its associations with landscapes across china," *Photogramm. Eng. Remote Sens.*, vol. 82, no. 2, pp. 135–148, 2016.
[60] W. R. Tobler, "A computer movie simulating urban growth in the Detroit region," *Econ. Geography*, vol. 46, no. sup1, pp. 234–240, 1970.
[61] H. J. Miller, "Tobler's First Law and Spatial Analysis," *Ann. Assoc. Amer. Geographers*, vol. 94, no. 2, pp. 284–289, 2004.
[62] A. S. Fotheringham, C. Brunsdon, and M. Charlton, *Geographically Weighted Regression: The Analysis of Spatially Varying Relationships*. Hoboken, NJ, USA: Wiley, 2003.
[63] F. Gao, W. Kustas, and M. Anderson, "A data mining approach for sharpening thermal satellite imagery over land," *Remote Sens.*, vol. 4, no. 11, pp. 3287–3319, 2012.

Quan Zhang received the M.S. degree in cartography and geography information system from Northwest University, Xi'an, China, in 2015, and the Ph.D. degree from Beijing Normal University, Beijing, China, in 2019.

He is currently working as a Postdoctor with the College of Urban and Environmental Science, Northwest University, Xi'an, China. His research interests include the retrieval, validation, scaling, and blending of remote sensed land surface temperature, and emissivity products.

Ninglian Wang received the M.S. and Ph.D. degrees from Cold and Arid Regions Environmental and Engineering Research Institute of Chinese Academy of Sciences (CAS), Beijing, China, in 1991 and 2001, respectively.

He performed Postdoctoral research work with Byrd Polar and Climate Research Center, Ohio State University, Columbus, OH, USA, during 2002–2003. He is currently a Professor at Northwest University, Kirkland, WA, USA. He is currently participating in the research work with the CAS Strategic Priority Research Program of Pan Third Pole Environment Study for a Green Silk Road (Pan-TPE). His research interests include climatic and environmental records in ice core, glacier changes and water resources, cryosphere, and global change.

Jie Cheng (Senior Member, IEEE) received the Ph.D. degree in cartography and remote sensing from the Institute of Remote Sensing Applications of Chinese Academy of Sciences, Beijing, China, in 2008. He was a Postdocotral Fellow with the State Key Laboratory of Remote Sensing Science, Beijing Normal University, Beijing, China, from 2008 to 2010, an Assistant Research Scientist with the University of Maryland, College Park, MD, USA, from 2009 to 2010, and a Visiting Scientist with the Hydrology and Remote Sensing Laboratory, United States Department of Agriculture-Agricultural Research Service, Beltsville, MD, USA, from 2017 to 2018.

He is currently an Associate Professor with the State Key Laboratory of Remote Sensing Science, Faculty of Geographical Science, Beijing Normal University, Beijing, China. He has authored or coauthed more than 60 SCI indexed peer-reviewed papers, seven book chapters, and two special issues of *Remote Sensing*. His main research interests include estimation of land surface variables from satellite observations, radiative transfer modeling, and studies on surface energy balance.

Shuo Xu received the B.S. degree in remote sensing science and technology from the Shandong University of Science and Technology, Qingdao, China, in 2014. She is currently working toward the M.S. degree in cartography and geographical information system at Beijing Normal University, Beijing, China. Her research interests mainly include the blending and validation of remote sensed land surface temperature.